Dist: A

REPORT DOCUMENTATION PAGE	1. REPORT NO. FINAL	2.	3. Recipient's Accession No. 1 Jul 93 - 31 Dec 93
4. Title and Subtitle Integrated Intelligent Structures for Suppressing Static Aerothermoelastic Deformations and Flutter of Panels			5. Report Date February 1994 Approved for public release, distribution unlimited
7. Author(s) Li-Chuan Chu		DTIC SELECTED FEB 0 1 1995 B NA	8. Performing Organization Rept. No. C & C TR 9401
9. Performing Organization Name and Address C & C Technologies, Inc. 1209 Botetourt Gardens Norfolk, Virginia 23517			10. Project/Task/Work Unit No. AFOSR-TR- 95 0053
			11. Contract(C) or Grant(G) No. (C) #F49620-93-C-0021 (G) 2302/DS
12. Sponsoring Organization Name and Address AFOSR 110 Duncan Ave. Bolling Air Force Base Washington, DC 20332			13. Type of Report & Period Covered Contractor Report (Final)
			14. Approved for public release, distribution unlimited A
15. Supplementary Notes Li-Chuan Chu (804) 622-3838			

16. Abstract (Limit: 200 words)
This document presents nonlinear panel flutter suppression study which has been accomplished by using both the finite element method and the classical continuum method. The results show that: (1) The bending moment is more effective than inplane force in active suppression using piezoelectric actuation. (2) The critical flutter dynamic pressure can be increased two to three times for the cases studied. (3) With embedded shape memory alloy (SMA) fibers, the critical buckling temperature of the composit panel is increased 10 to 20 times that of the panel with no SMA, and the static aerothermoelastic deformation is eliminated. (4) Flutter stability region is enlarged significantly with SMA. (5) Panel flutter suppression for integrated composite structures can be achieved effectively by using piezoelectric materials at low temperatures and SMA at high temperatures.

17. Document Analysis a. Descriptors

b. Identifiers/Open-Ended Terms
Intelligent structures
Panel flutter
Active/passive control
Composite plate
c. COSATI Field/Group

DISTRIBUTION STATEMENT A
Approved for public release
Distribution Unlimited

18. Availability Statement C & C Technologies, Inc. 1209 Botetourt Gardens Norfolk, Virginia 23517	19. Security Class (This Report) Unclassified	21. No. of Pages 29
	20. Security Class (This Page) Unclassified	22. Price

(See ANSI-Z39.18)　　　　　　　　　　　　　　　　　OPTIONAL FORM 272 (4-77)

DTIC QUALITY INSPECTED 3

19950130 050

i

Table of Contents

SUMMARY

The contents of this report serve to fulfill the requirements of the Phase I SBIR contract #F49620-93-C-0021 between AFOSR/PKC and C & C Technologies, Inc. entitled "Integrated Intelligent Structures for Suppressing Static Aerothermoelastic Deformations and Flutter of Panels". The ultimate goal of this project is to develop a commercial package of methodology, information, and criteria, along with documented computer programs, for designing integrated intelligent panel structures to meet static aerothermoelastic deformation and flutter requirements. To accomplish this we have, in Phase I, investigated the properties and behaviors of integrated intelligent structures consisting of advanced composite laminates, embedded shape memory alloys (SMA) and piezoelectric materials, and two dynamic control systems. In this Final Technical Report, the results of the Phase I effort are presented in detail to demonstrate achievement of the objectives of the project and to show how this innovative integrated intelligent structure can be fully exploited in Phase II and beyond.

By successfully meeting or exceeding all of the Phase I objectives, we have: (1) Designed optimally shaped piezoelectric actuator configurations and two linear controllers for active flutter suppression; (2) Synthesized a simple model-independent signature-based controller using collocated sensor/actuator for suppressing nonlinear flutter motion; (3) Developed constitutive relations for thermally stressed composite laminates with embedded shape memory alloys for suppressing static aerothermoelastic deformations and passive flutter control; (4) Demonstrated panel flutter suppression through simulations using integrated piezoelectric active control and SMA passive control for laminated composite panels; and (5) Included large-deflection nonlinearity in the control simulations.

In Phase I, nonlinear panel flutter suppression has been studied by using both the finite element method and the classical continuum method. The results show that (1) The bending moment is more effective than inplane force in active flutter suppression using piezoelectric actuation. (2) With a pair of small piezoelectric layers patched at the leading edge, the critical dynamic pressure can be increased about three times by using linear optimal control and increased about two times by using the model-independent signature-based control. (3) With embedded SMA fibers, the critical buckling temperature of the composite panel is increased 10 to 20 times that of the panel with no SMA, and the static aerothermoelastic deformation is eliminated. (4) Flutter stability region is enlarged significantly with SMA. (5) Panel flutter suppression for integrated composite structures can be achieved effectively by using piezoelectric materials at low temperatures and SMA at high temperatures.

NOMENCLATURE

A_n = modal amplitude

D = plate bending stiffness

E = Young's modulus

G = Shear modulus

M_∞ = Mach number

Nc = number of the actuator sets

M_k, N_k = moment and inplane force in k-th direction

V_∞ = free stream airflow speed

Q = positive semi-definite state penalty matrix

R = positive definite control penalty matrix

T = operation temperature

ΔT = temperature change

Φ = Airy stress function

a_n = nondimensional modal amplitude

a = panel length

b = panel width

c_a = nondimensional aerodynamic damping

d_{ij} = mechanical and electric coupling coefficient

e = electric field

h = panel thickness

p-p_∞ = aerodynamic pressure

t, τ = time and nondimensional time

w = transverse panel deflection

x = streamwise coordinate

y = spanwise coordinate

z = normal coordinate

v = Poisson's ratio

ρ = density

σ, τ_{xy} = stresses

$\in, \gamma_{xy}$ = strains

λ = nondimensional dynamic pressure

$[A_a]$ = system aerodynamic influence matrices

$[K]$ = system stiffness matrices

[M]	=	system mass matrices
[G]	=	system aerodynamic damping matrices
g_a	=	nondimensional aerodynamic damping factor
fp,fv	=	scale factors for the position and velocity sensors
kp,kv	=	position and velocity feedback gains
A_s	=	austenite start temperature
A_f	=	austenite finish temperature
[N1],[N2]	=	the first and second nonlinear stiffness matrices
[W]	=	panel deflection

Subscripts

a	=	air
b	=	bending
cr	=	critical
m	=	membrane
max	=	maximum
p	=	piezoelectric material
s	=	base structure
ΔT	=	temperature change

I. INTRODUCTION

Panel flutter at supersonic speeds has been encountered in the operation of aircraft and missiles. Panel flutter differs from the conventional lifting surface or wing flutter in at least three important respects: (1) it is entirely a supersonic/hypersonic phenomenon; (2) the airflow is only on one side of the panel; and (3) the structural nonlinearities due to large transverse deflections of panels tend strongly to exhibit large-amplitude limit-cycle oscillations.

The earliest reported structural failures that could be attributed to panel flutter were the failure of the 60 to 70 early German V-2 rockets during World War II [1, 2]. A most recent panel flutter failure was reported by Rick Baker, F-117A Deputy Chief Engineer, Lockheed-Burbank in his keynote address at the AIAA Dynamics Specialist Conference [3]. After the flight tests of the F-117A Stealth Fighter, cracks due to flutter were found in almost half of the laminated composite skin panels. Those panels were redesigned and stiffened and thus a tremendous weight penalty was paid. The additional weight resulted in

smaller payloads and reduced flight speeds, and hindered aircraft maneuverability, which is extremely important for fighter aircraft during combat.

At present, a variety of high speed flight vehicles are either under development or being considered for development such as the YF-22 Advanced Tactical Fighter (ATF), the National Aero-Space Plane (NASP), and the High Speed Civil Transport (HSCT). All these vehicles feature increased performance in comparison with currently existing aircraft. Improvement in performance characteristics such as higher speeds (Mach numbers), greater maneuverability, larger payload and increased efficiency can be expected to lead to new panel flutter problems arising from higher dynamic pressure loads (or airflow speed), higher temperatures and large deflections of light weight composite structures. When a flight vehicle travels at high speeds, the onset of flutter may be imminent but usually the dynamic pressure is not the only form of excitation. An aircraft panel is subjected to combined aerodynamic pressure and thermal loads. The friction from the surrounding air causes increased heating of the structure. The presence of high temperature loads results in flutter motions at dynamic pressures much lower than when there are no thermal effects [4-8]. This would result in lower flight speed limits. In addition, the temperature rise may also cause large aerodynamic-thermal deflections of the skin panels. This distortion in shape from the original configuration alters the lift-to-drag characteristics of the aircraft and may thus lead to poor performance.

II. PHASE I TECHNICAL OBJECTIVES

The ultimate goal of this project is to develop a commercial package of methodology, information, and criteria, along with documented computer programs, for designing integrated intelligent panel structures to meet static aerothermoelastic deformation and flutter requirements. To accomplish this we have, in Phase I, investigated the properties and behaviors of integrated intelligent structures consisting of advanced composite laminates, embedded shape memory alloys (SMA) and piezoelectric materials, and two dynamic control systems. Specific objectives include: (1) Initiate panel flutter analysis of intelligent structures, including intelligent actuator design using piezoelectric materials; (2) Study the implementation of linear optimal controller design and model-independent signature-based controller design; (3) Study the design of intelligent actuators using shape memory alloys; (4) Perform integrated design and development of actively-controlled intelligent-structure panels for flutter suppression.

III. ACTIVE CONTROL WITH PIEZOELECTRIC MATERIALS

1. Mathematical Formulation

1A. Classical Continuum Method

Piezoelectric materials can develop an electrical charge when subjected to a mechanical strain. The converse piezoelectric effect, the development of mechanical strain when subjected to an electrical field, can be utilized to actuate a structure and induce inplane forces and bending moments. Thus, actuation of a structure may be accomplished at the material level. The basic electric-mechanical stain and stress relation is

$$\begin{Bmatrix} \sigma_x \\ \sigma_y \\ \tau_{xy} \end{Bmatrix} = \frac{E_p}{1-v_p^2} \begin{bmatrix} 1 & v_p & 0 \\ v_p & 1 & 0 \\ 0 & 0 & \frac{1}{2}(1-v_p) \end{bmatrix} \left(\begin{Bmatrix} \epsilon_x \\ \epsilon_y \\ \gamma_{xy} \end{Bmatrix} - e_3 \begin{Bmatrix} d_{31} \\ d_{32} \\ 0 \end{Bmatrix} \right). \tag{1}$$

In order to use the classical method to investigate the panel flutter problem, we assume that (a) the piezoelectric material used here is isotropic; (b) the piezoelectric material covers the entire top and bottom surfaces of the panel; and (c) the inplane forces induced by the piezoelectric actuators are uniform. The piezoelectric materials will produce bending moments and inplane forces depending upon the electric field applied by the controller. These inplane forces and bending moments would increase the critical dynamic pressure. Since the present work is concerned with modification of the structural behavior rather than aerodynamic precision, the first-order-piston-theory-type relation which is expressed in Eq. (2) is considered to provide an adequate representation of the supersonic aerodynamic loads. Consequently, the loads are obtained from the relation

$$p - p_\infty = \frac{2q}{\beta} \left(\frac{\partial w}{\partial x} + (\frac{M_\infty^2 - 2}{M_\infty^2 - 1}) \frac{1}{V_\infty} \frac{\partial w}{\partial t} \right), \tag{2}$$

where $q = \frac{1}{2}\rho_\infty V_\infty^2$ is the dynamic pressure, and $\beta = \sqrt{M_\infty^2 - 1}$. The nondimensional dynamic pressure is given by $\lambda = \frac{2qa^3}{\beta D}$. Another commonly used nondimensional parameter is the mass ratio which is defined as $\mu = \frac{\rho_\infty a}{m_0}$ where m_0 is the average mass density of panel.

The piezoelectric laminates are placed symmetrically with respect to the midplane, so

that bending and stretching deformations are decoupled. We also assume that Poisson's ratio is the same for both materials, i.e. $\nu_s = \nu_p = \nu$, consequently the nonlinear equations of motion can be greatly simplified as,

$$D\nabla^4 w = \frac{\partial^2 \Phi}{\partial y^2}\frac{\partial^2 w}{\partial x^2} + \frac{\partial^2 \Phi}{\partial x^2}\frac{\partial^2 w}{\partial y^2} - 2\frac{\partial^2 \Phi}{\partial x \partial y}\frac{\partial^2 w}{\partial x \partial y} + N_x^0 \frac{\partial^2 w}{\partial x^2} + N_y^0 \frac{\partial^2 w}{\partial y^2} -$$
$$-(p - p_\infty) - m_0 \frac{\partial^2 w}{\partial t^2} - \sum_{i=1}^{Nc} e_{bi}\left[R_{31}J_{i1} + R_{32}J_{i2}\right], \tag{3}$$

$$\frac{1}{Eh}\nabla^4 \Phi = \left(\frac{\partial^2 w}{\partial x \partial y}\right)^2 - \left(\frac{\partial^2 w}{\partial x^2}\right)\left(\frac{\partial^2 w}{\partial y^2}\right), \tag{4}$$

where the definitions of variables (see Nomenclature) follow those of reference [9]. For the panel flutter analysis, only the first spanwise mode is considered. The flutter deflection of a simply supported plate can then be approximated by

$$w = \sum_n A_n \sin\left(\frac{n\pi x}{a}\right)\sin\left(\frac{\pi y}{b}\right). \tag{5}$$

By using Galerkin's method, the governing ordinary nonlinear differential equation in nondimensional form becomes [9]

$$\mathbf{M}\frac{d^2\mathbf{Z}}{d\tau^2} + \mathbf{C}\frac{d\mathbf{Z}}{d\tau} + (\mathbf{K}_s + \mathbf{K}_p U_m + \mathbf{K}_a \lambda + \mathbf{K}_{qq})\mathbf{Z} = \mathbf{G}\mathbf{U}_b, \tag{6}$$

where $\mathbf{Z}$ is the vector of generalized coordinates $a_n(= A_n / h)$, τ is a nondimensional time, $\mathbf{K}_{qq}$ is the nonlinear stiffness matrix, U_m and $\mathbf{U}_b$ are normalized control variables for inplane force and bending moment respectively, and other terms are straight forward. It is noted that

$$\begin{Bmatrix} U_m \\ \mathbf{U}_b \end{Bmatrix} = \frac{1}{e_{3max}}\begin{Bmatrix} e_m \\ \mathbf{e}_b \end{Bmatrix}, \tag{7}$$

where e_{3max} is the maximum operating electric field of the piezoelectric material. Because of the e_{3max} limitation, for a given U_m, there is a constraint for the normalized control variable

$$|U_{bi}| \le 1 - |U_m|. \tag{8}$$

1B. Finite Element Method

Using the finite element approach, the panel can be studied for more complicated

geometries, support conditions and composite-laminate arrangements. The nonlinear finite element equations of motion are derived from the principle of virtual work. For a laminated aircraft panel consisting of fiber-reinforced composite and piezoelectric layers subjected to a temperature change of $\Delta T(x,y,z)$, the system equations of motion are given by

$$\frac{1}{\omega_0^2}[M]\{\ddot{W}\} + \frac{1}{\omega_0}[C]\{\dot{W}\} + (\lambda[A_a] + [K] - [K_{N\Delta T}] - [K_{Ne}] + [N1] + [N2])\{W\} = \{P_{\Delta T}\} + \{P_e\}$$

(9)

where the definitions of symbols (see Nomenclature) follow those of reference [10]. Because of the large number of degrees-of-freedom usually involved with finite element model, Eq. (9) is not suitable for control to suppress the panel deflection $\{W\}$. A modal-coordinate transformation, therefore, is used to convert it to a reduced number of modal coordinates. The resulting reduced second-order equation is shown in Eq. (6). Numerical results for nonlinear panel flutter motions obtained from the classical continuum method previously described validate results obtained from the finite element method.

2. Piezoelectric Actuator Configuration Design

A typical laminated aluminum panel, shown in Figure 1, contains two piezoelectric layers of equal thickness placed symmetrically with respect to the midplane of the panel. The actuator set can be stimulated such that one laminate contracts and the other expands to create bending moments in the structure, such that both layers exhibit the same strain resulting in nonzero inplane forces, or a combination of the two. Both induced bending moments and inplane tensile forces can increase the stiffness of the controlled structure.
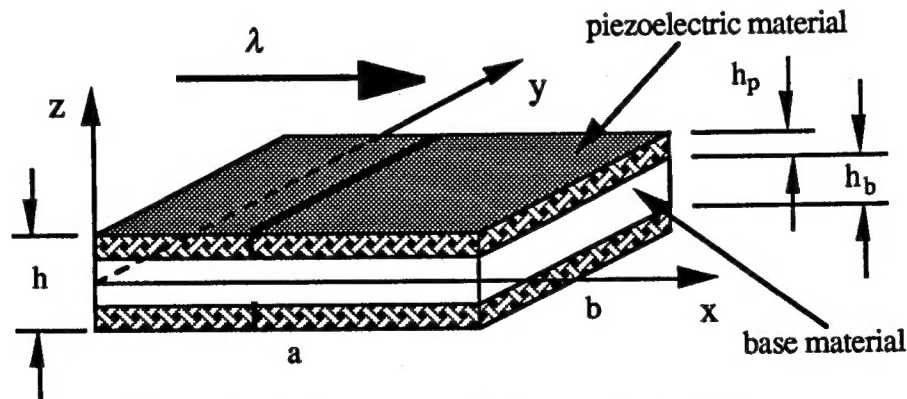

Fig. 1 Panel Geometry with Piezoelectric Layers.

Figure 2 shows three piezoelectric actuator arrangements considered in Phase I. They are: *one-set patched, two-set patched,* and *one-set small patched* embedded piezoelectric

laminates. In the first two configurations, an isotropic panel is completely covered by the piezoelectric layers. For the two-set piezoelectric actuator configuration, each set actuator can be activated by different controller. Note that the one-set configuration is a limiting case of the two-set configuration. In the last configuration only a small part of the top and bottom layers of an eight-layer composite panel is embedded with piezoelectric materials adjacent to the leading edge.
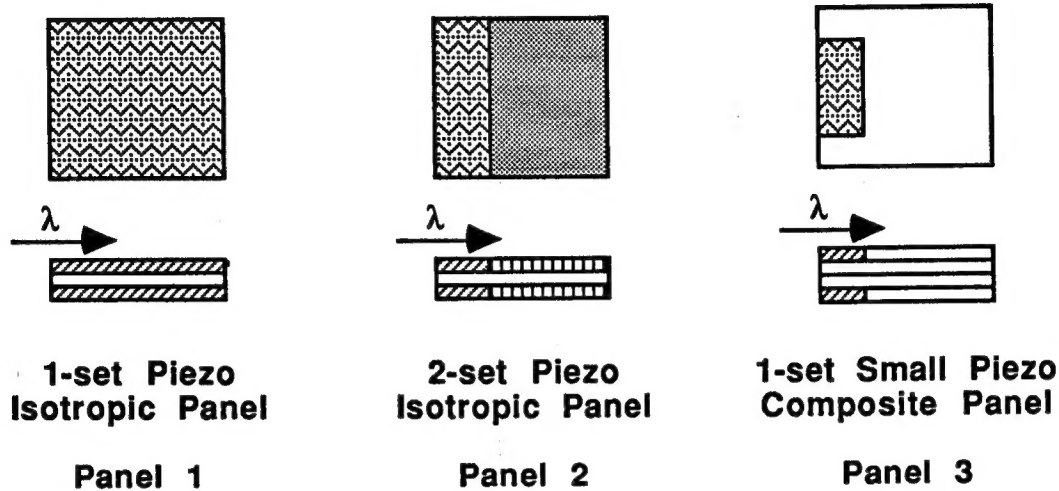

1-set Piezo Isotropic Panel

Panel 1

2-set Piezo Isotropic Panel

Panel 2

1-set Small Piezo Composite Panel

Panel 3

Fig. 2 Piezoelectric Actuator Configuration Design.

3. Linear Control Designs

3A. Linear Optimal Control

For the suppression of panel flutter, an optimal control approach based on the linear optimal control theory is considered first. The control design is based on the linear model obtained by ignoring the nonlinear term of Eq. (6). For optimal control using both inplane forces and bending moments, the stiffness matrix varies with U_m . The problem can be simplified by first assuming U_m to be a constant. The control variable then becomes U_b which induces bending moment only. From Eq. (6), the first order dynamic equation becomes

$$\frac{d\mathbf{X}}{d\tau} = \mathbf{AX} + \mathbf{BU} ,$$

(10)

where

$$\mathbf{X} = \begin{bmatrix} \mathbf{Z} \\ \frac{d\mathbf{Z}}{d\tau} \end{bmatrix}, \quad \mathbf{A} = \begin{bmatrix} 0 & \mathbf{I} \\ -\mathbf{M}^{-1}\left(\mathbf{K}_s + \mathbf{K}_p U_m + \mathbf{K}_a \lambda\right) & -\mathbf{M}^{-1}\mathbf{C} \end{bmatrix}, \quad \mathbf{B} = \begin{bmatrix} 0 \\ \mathbf{M}^{-1}\mathbf{G} \end{bmatrix}, \quad \mathbf{U} = \mathbf{U}_b.$$

The linear quadratic performance index for optimal control can be formulated as

$$J = \frac{1}{2} \int_0^\infty (X^T Q X + U^T R U) d\tau,$$ (11)

where Q is a positive semi-definite state penalty matrix and R is a positive definite control penalty matrix. From the optimal control theory, the optimal controller for this linear quadratic regulator problem is obtained by

$$U = -R^{-1} B^T P X,$$ (12)

where P is a positive definite matrix obtained from the following Riccati equation [10]

$$A^T P + P A - P B R^{-1} B^T P = -Q.$$ (13)

The weighting matrix R is chosen as an identity matrix times a positive constant, and the weighting matrix Q is chosen by the energy weighting method in this study

$$Q = \begin{bmatrix} K_s & 0 \\ 0 & M \end{bmatrix}.$$ (14)

For a different constant U_m, an optimal feedback control gain for U_b can be obtained. Through numerical simulations using nonlinear equations of the panel, the critical dynamic pressure can be obtained. Finally, an optimal set of U_m and U_b is obtained by comparing the results obtained from different constant U_m.

3B. Model-Independent Signature-Based Control

In this section, we study the feasibility of the model-independent signature-based control design. For linear optimal control, we need full state feedback and an accurate model to design the controller. In general, it is very difficult to design a set of sensors to measure all the states which include the position and velocity of each mode. If the full state information can not be directly obtained from sensors, we need a state estimator to estimate all the states indirectly. On the other hand, an accurate model is also very difficult to obtain. Either the state estimation error or the modeling error may degrade the performance of the controller. This motivates us to design the model-independent signature-based controller to avoid these two problems. The term *model-independent* means that the feedback gains in the controller design can be determined without any model information. Output feedback is used to replace the state feedback. The term *signature-based* means that the model is still important to decide the optimal locations for collocated sensors/actuators.

This controller design is very similar to the passive damping and stiffness design for structural systems [11]. As we know, when a mass-spring-dashpot is attached to any mechanical system, the damping and stiffness of the system are almost always augmented and the stability of the system is thus improved. The question arises as to whether there are any feedback control designs using sensors and actuators which behave like the passive mass-spring-dashpot. These kinds of controllers sometimes are called virtual passive controllers and can be achieved by using collocated sensors/actuators and direct negative feedback controls. Recall a simplified linear model equation from Eq. (6)

$$M\ddot{Z} + C\dot{Z} + KZ = GU. \tag{15}$$

For collocated sensors/actuators and a direct negative feedback control, one has

$$Y = \begin{bmatrix} y_p \\ y_v \end{bmatrix} = \begin{bmatrix} f_p G^T Z \\ f_v G^T \dot{Z} \end{bmatrix}$$

$$U = -\begin{bmatrix} k_p & k_v \end{bmatrix} Y = -(f_p k_p G^T Z + f_v k_v G^T \dot{Z}). \tag{16}$$

where f_p and f_v are scale factors for the position and velocity sensors, respectively, and k_p and k_v are position and velocity feedback gains, respectively. The closed-loop linear system becomes

$$M\ddot{Z} + \left(C + f_v k_v G^T\right)\dot{Z} + \left(K + f_p k_p G^T\right)Z = 0. \tag{17}$$

The augmented damping $f_v k_v G^T$ and stiffness $f_p k_p G^T$ depend on k_v, k_p and G. Larger k_v and k_p can provide larger damping and stiffness but need larger control power. Meanwhile, G depends on the size, shape and location of the collocated sensors/ actuators. To achieve proper augmented damping and stiffness for suppressing the panel flutter, we have to find the best G by investigating all possible configurations of the collocated sensors/actuators. The knowledge of the model can be used for the optimal sensors/actuators configuration design.

4. Numerical Results

4A. Results for Isotropic Panel

In this section, numerical results are presented for suppressing flutter of an isotropic panel using the linear optimal control and the model-independent signature-based control. The panel studied is a simply supported square aluminum panel with two piezoelectric

laminates which cover the two surfaces of the panel (Panel 1 of Fig. 2). The physical parameters and the geometry of the panel are shown in Appendix.

First, optimal control design is performed. Figure 3 shows time response of the maximum panel deflection and the feedback control effort. The nondimensional dynamic pressure λ is 1400, and the inplane force is set to zero. Time response of the panel deflection shows a limit cycle motion at the beginning. After the controller is activated, the panel deflection is quickly suppressed.

The inplane force can change the panel stiffness. Inplane tension increases the stiffness, and inplane compression decreases the stiffness. Figure 4 shows the inplane force effect on the λ_{cr} with or without bending moment used for optimal feedback control. The range of control authority for bending moment varies with the inplane force. When the inplane force is set to the maximum or minimum value, no bending moment can be induced because of the limitation shown in Eq. (8). As the inplane force approaches zero, the λ_{cr} increases dramatically, and the flutter free region is enlarged. With zero control of inplane stress and maximum control of bending moment, the λ_{cr} can be increased to three times the value for the uncontrolled panel. Control of the bending moment is obviously the more effective way to suppress flutter.

The one-set patched actuator is an extreme case of the two-set patched actuator (Panel 2 in Fig. 2). If normalized separating position is set to 0 or 1, then the two-set patched actuator becomes a one-set patched actuator. Figure 5 shows the variation of λ_{cr} with the normalized separation position of a two-set patched actuator and the control weighting factor r. The inplane force is set to zero. The result shows that the two-set actuator can perform better than a one-set actuator. Table 1 also shows that if only the first set is activated (x/a = 0.3, for example), the λ_{cr} still can be increased more than three times the value 514 for the uncontrolled panel. In fact, one-set activated with x/a as low as 0.3 is more effective than with x/a = 1.0 (i.e., equivalent to Panel 1).

Optimal location for small patched actuators is also studied by analyzing the norm of the optimal feedback gain at various locations of the panel (see Fig. 6). The finite element model is meshed by 10x6 rectangular elements. The nondimensional dynamic pressure is 1000. Numerical results show that if the actuator is patched at the locations with higher norm, it can suppress flutter more effectively. If the piezoelectric materials are patched at the locations with the norms higher than 120 (adjacent to the leading edge), the critical dynamic pressure can be increased about four times of the value without piezoelectric actuation.
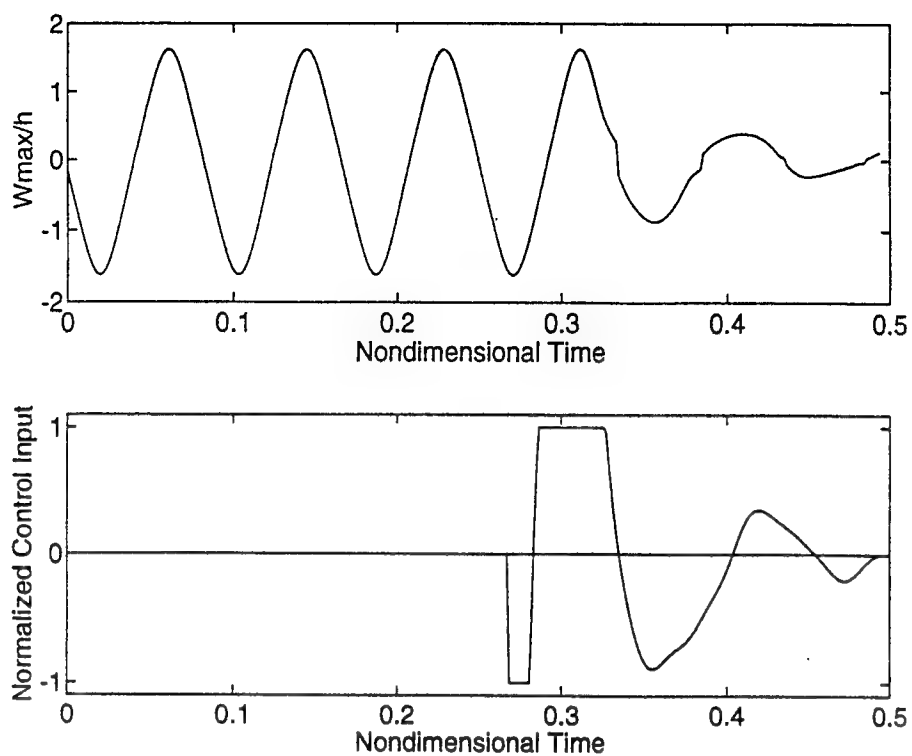
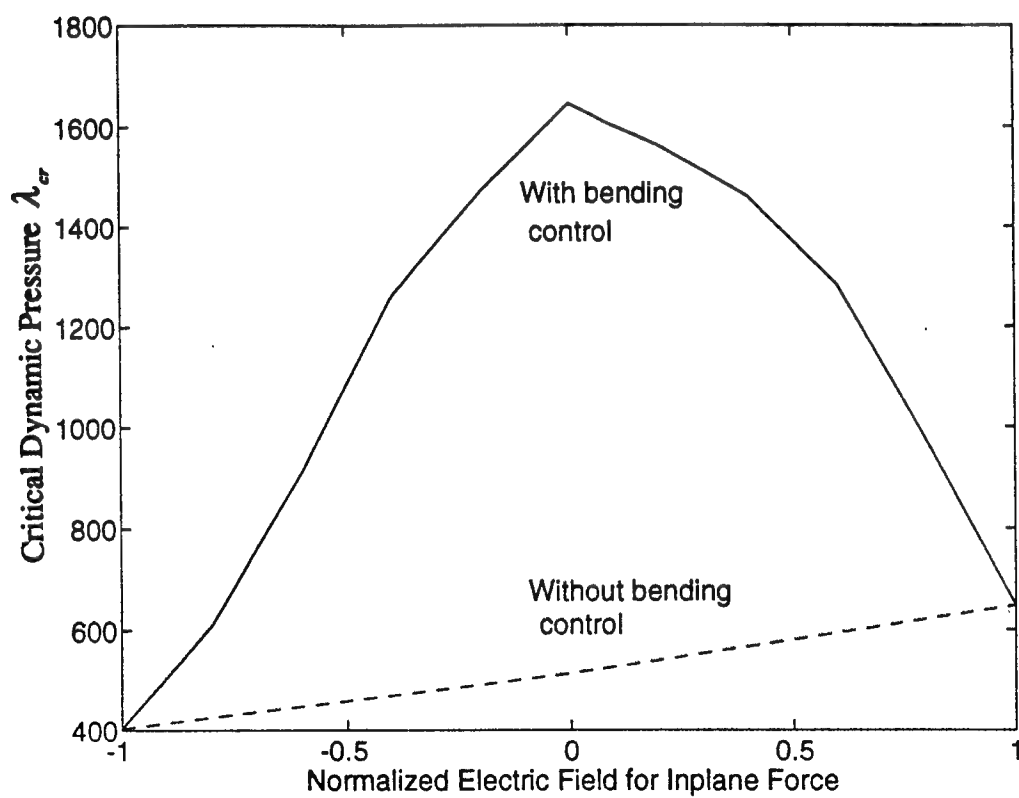Fig. 3 Time History of Panel Deflection and Control Effort.

Fig. 4 Critical Dynamic Pressure λ_{cr} with/without Bending Moment Control.
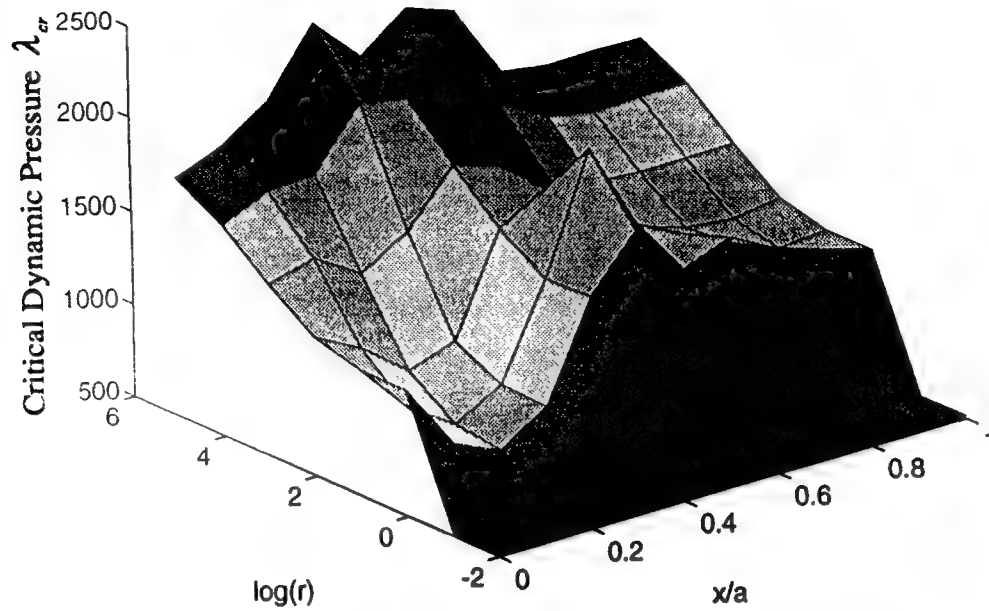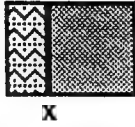
Fig. 5 Critical Dynamic Pressure λ_{cr} vs. Normalized Separating Position (x/a) and Control Weighting Factor r for a Two-Set Patched Actuator.

Table 1 Comparison of λ_{cr} for 2-Set Piezo, Isotropic Panel, with $\mathbf{R} = 10,000 \times \mathbf{I}$

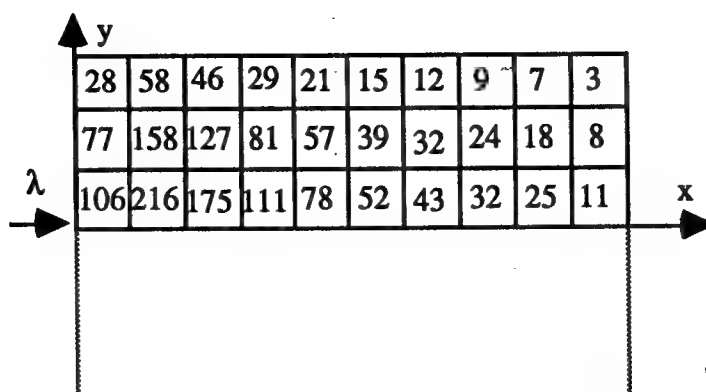|	x/a	λ_{cr}	$\lambda_{cr}/514$
Only First Set is Activated	0.1	875	1.7
	0.2	1536	3.0
	0.3	1790	3.5
	0.4	1814	3.5
	0.5	1768	3.4
	1	1647	3.2
Both Sets are Activated	0 or 1	1545	3.0
	0.3	1862	3.6

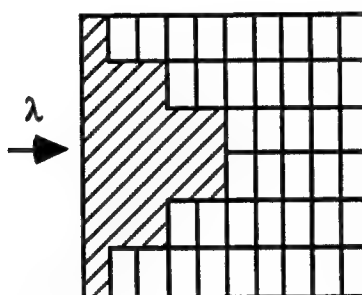Fig. 6. Norm of the Optimal Feedback Gain for Upper Half Panel

Fig. 7. Optimal Collocated Sensor/Actuator Configuration (Shaded Part) for Model-
Independent Signature-Based Control.

Next, the model-independent signature-based control design is studied. The finite
element model is meshed by 10x6 rectangular elements. Optimal sensor/actuator locations
(see Fig. 7) are obtained by investigating all possible configurations of the collocated
sensors/actuators. The feedback gains are not only model independent but also
aerodynamic independent. The result shows that the nondimensional critical dynamic
pressure can be increased from 514 up to about 1100.

Since this model-independent controller does not require the knowledge of the model
and the state information, it is very simple and attractive for experimental validation in
Phase II. However, the design of the size, shape and location of the collocated sensors/
actuators to maximize the critical dynamic pressure needs further study by using the
knowledge of the model. A new finite element analysis based on triangular elements
instead of rectangular also needs to be developed to further improve the sensor/actuator

configuration.

4B. Results for Composite Panel

A simply supported square thin composite panel is studied. The panel is of dimension 12"x12"x0.05", and is made up of eight layers with lamination angle [0/45/-45/90]$_s$. All inplane displacements are considered to be zero at the edges (u=v=0). The material properties for the panel are shown in Appendix. A one-set small patched piezoelectric layer is embedded within the composite top and bottom 0-deg. layers (see Fig. 2). These piezoelectric layers have an isotropic behavior. Their properties are also shown in Appendix.

The panel is modeled by a 10x6 array of C^1 conforming rectangular bending element. The modal equation of motion, Eq. (6), is solved by Runge-Kutta method. The inplane forces induced by the piezoelectric layers are null, since the voltages applied on top and bottom piezoelectric patches are with the same values but different signs. Figure 8 plots the maximum panel deflection vs. nondimensional dynamic pressure for different numbers of modes retained in Eq. (6). The six-mode representation appears to give a converged limit-cycle result.
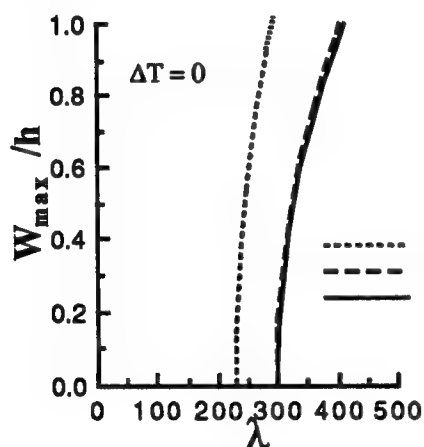

Fig. 8 Maximum Panel Deflection with
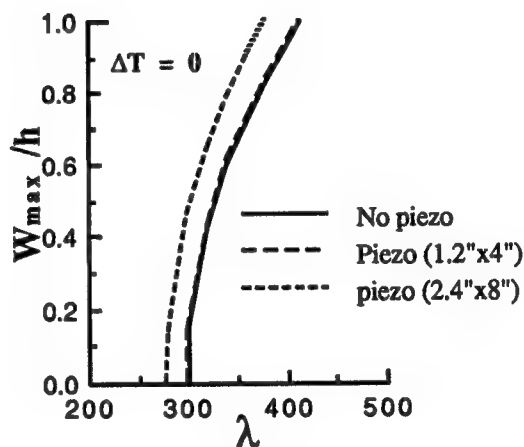Different Number of Modes.

Fig. 9 Maximum Panel Deflection with
Different Piezo Sizes.

The effect of the embedded piezoelectric actuator size has also been studied (Panel 3 in Fig. 2), and the results are illustrated in Fig. 9. The larger the inactive piezo patch, the lower the dynamic pressure is, because inclusion of piezoelectric materials reduces the panel stiffness. However, if piezoelectric actuator is activated using linear optimal control,

the critical dynamic pressure can be increased from 279 to 686 for the 2.4"x8" piezo size and from 298 to 429 for the 1.2"x4" piezo size. The optimal shape and size of the piezoelectric actuator will be studied in Phase II.

IV. PASSIVE CONTROL WITH SMA

It is known that the compressive thermal stresses induced by high temperature generally reduce panel stiffness and hence reduce the critical dynamic pressure. Lower speed-limit of the aircraft could result. This is illustrated in Fig. 10 for the same laminated panel discussed in the previous section but without piezoelectric material. Shape memory alloys (SMA), however, have three interesting features in a thermal environment. When an initially strained elongated SMA fiber is heated above its characteristic transformation (austenite finish A_f) temperature, it will: (1) return to its original length or produce a recovery tensile stress in the fiber with an edge-immovable (strain restrained) boundary; (2) increase its Young's modulus by a factor of three or four; and (3) greatly increase its yielding strength. These characteristics are shown in Fig. 11 [12] for 55-Nitinol alloy.

The aerodynamic heating exerted on the skin panels of a supersonic vehicle will cause panel temperatures well above the austenite finish temperature A_f. Thus the three features of the SMA will be ideal for passive control of flutter by embedding the SMA fibers in a laminated composite panel. The SMA will reduce the adversary thermal stress effects on panel flutter and increase the critical dynamic pressure of the panel.

1. Mathematical Formulation

In previous studies of SMA reinforced composites [14,15], the thermal stress effect in the composite matrix was neglected. For the application of SMA in a thermal environment, this effect has to be considered in the formulation. The constitutive equation for a composite laminate with embedded SMA fiber, which includes the thermal effects, is developed in this study.

1A. Properties of a Composite Lamina with Embedded SMA Fibers

The stress-strain relations of a composite lamina (for example, graphite-epoxy) with embedded SMA fibers in material principal directions are [16]
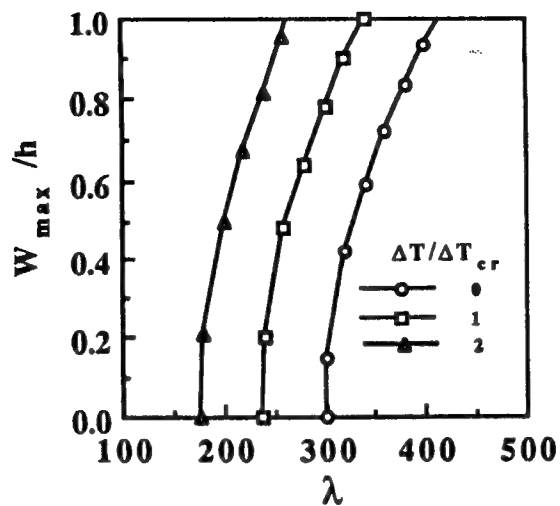
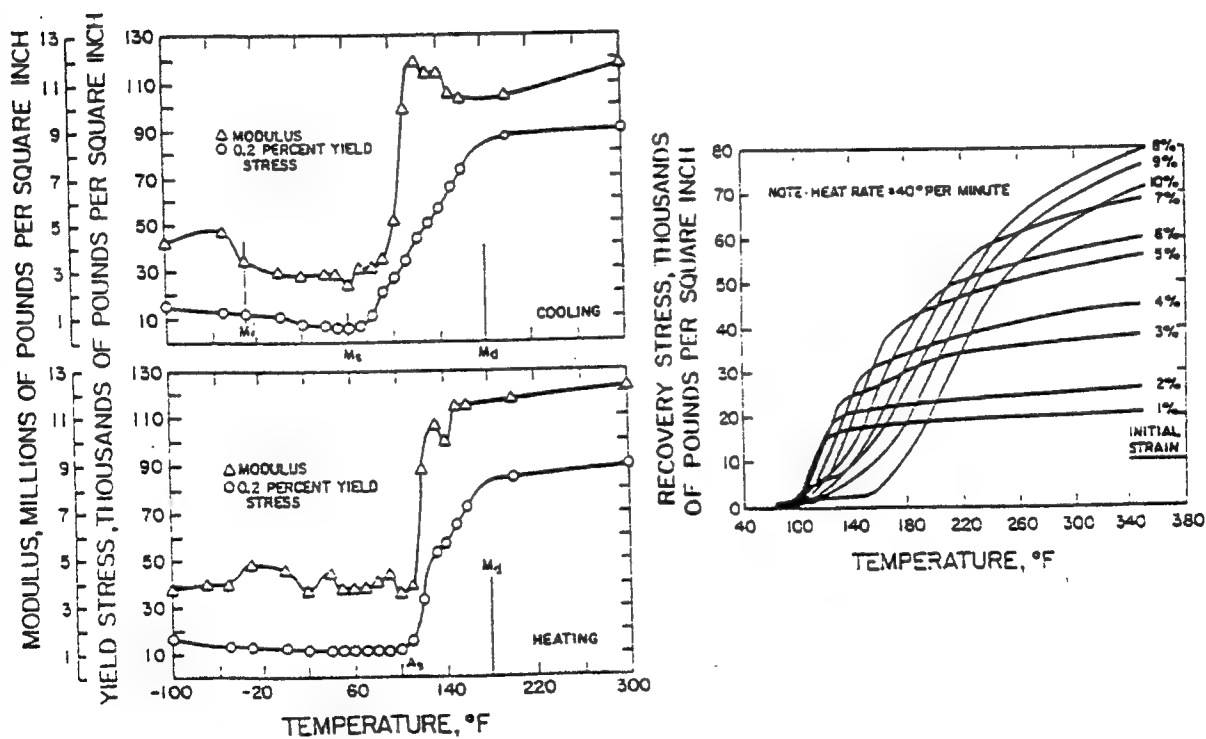Fig. 10 Limit-Cycle Amplitude of a Thermally Loaded, Simply Supported, Laminated Panel.

Fig. 11 Shape Memory Alloy Material Property.

$$\begin{Bmatrix} \sigma_1 \\ \sigma_2 \\ \tau_{12} \end{Bmatrix} = [Q]^* \left(\begin{Bmatrix} \varepsilon_1 \\ \varepsilon_2 \\ \gamma_{12} \end{Bmatrix} - \begin{Bmatrix} \alpha_1 \\ \alpha_2 \\ 0 \end{Bmatrix} \Delta T \right), \quad \text{for } T<A_S \qquad (18)$$

and

$$\begin{Bmatrix} \sigma_1 \\ \sigma_2 \\ \tau_{12} \end{Bmatrix} = [Q]^* \begin{Bmatrix} \varepsilon_1 \\ \varepsilon_2 \\ \gamma_{12} \end{Bmatrix} - [Q_m] \begin{Bmatrix} \alpha_{1m} \\ \alpha_{2m} \\ 0 \end{Bmatrix} V_m \Delta T + \begin{Bmatrix} \sigma_r^* V_s \\ 0 \\ 0 \end{Bmatrix}, \quad \text{for } T>A_S \qquad (19)$$

where the reduced stiffness matrix $[Q_m]$ is evaluated by E_{1m}, E_{2m}, G_{12m}, and ν_{12m} of the composite matrix, and V_m and V_s are volume fractions of composite matrix and SMA fibers. The reduced stiffness matrix $[Q]^*$ is evaluated by E_1, E_2, G_{12}, and ν_{12} of the SMA reinforced composite [16],

$$\alpha_1 = \frac{E_{1m} V_m \alpha_{1m} + E_s^* V_s \alpha_s}{E_{1m} V_m + E_s^* V_s}, \quad (E_1, \nu_{12}) = (E_{1m}, \nu_{12m}) V_m + (E_s^*, \nu_s) V_s,$$

$$\alpha_2 = V_m \alpha_{2m}, \qquad (E_2, G_{12}) = \frac{(E_{2m} E_s^*, G_{12m} G_s^*)}{[(E_{2m}, G_{12m}) V_s + (E_s^*, G_s^*) V_m]}. \qquad (20)$$

The superscript (*) indicates that the quantity is temperature dependent, and the recovery stress σ_r^* of SMA depends on the temperature as well as the initial strain ε_r (Fig. 11).

For a general k-th layer of lamination angle θ, the stress-strain relations in laminate coordinates become

$$\{\sigma\}_k = \begin{Bmatrix} \sigma_x \\ \sigma_y \\ \tau_{xy} \end{Bmatrix}_k = [\overline{Q}]_k^* \left(\begin{Bmatrix} \varepsilon_x \\ \varepsilon_y \\ \gamma_{xy} \end{Bmatrix} - \begin{Bmatrix} \alpha_x \\ \alpha_y \\ \alpha_{xy} \end{Bmatrix}_k \Delta T \right), \quad \text{for } T<A_S \qquad (21)$$

and

$$\{\sigma\}_k = [\overline{Q}]_k^* \begin{Bmatrix} \varepsilon_x \\ \varepsilon_y \\ \gamma_{xy} \end{Bmatrix} - [\overline{Q}_m]_k \begin{Bmatrix} \alpha_{xm} \\ \alpha_{ym} \\ \alpha_{xym} \end{Bmatrix}_k V_m \Delta T + \begin{Bmatrix} \sigma_{xr}^* \\ \sigma_{yr}^* \\ \tau_{xyr}^* \end{Bmatrix} V_s, \quad \text{for } T>A_S. \qquad (22)$$

The resultant stress are defined as

$$\{N, M\} = \int_{-h/2}^{h/2} \{\sigma\}_k (1, z) dz. \qquad (23)$$

1B. Finite Element Equations of Motion

By using the principle of virtual work, the governing equations of motion are derived for the panel flutter with the effects of thermal and SMA recovery stresses as,

$$\frac{1}{\omega_o^2}[M]\{\ddot{W}\} + \frac{g_a}{\omega_o}[G]\{\dot{W}\} + (\lambda[A_a]+[K]-[K_{N\Delta T}]$$
$$+[K_\sigma]+\tfrac{1}{2}[N1]+\tfrac{1}{3}[N2])\{W\} = \{P_{\Delta T}\}-\{P_\sigma\}, \tag{24}$$

where $[G]$ and $[A_a]$ are the aerodynamic damping and influence matrices, $[K_{N\Delta T}]$ and $[K_\sigma]$ are the thermal geometric and SMA recovery stress stiffness matrices, $[N1]$ and $[N2]$ are the first and second order nonlinear stiffness matrices, and $\{P_{\Delta T}\}$ and $\{P_\sigma\}$ are the thermal load and SMA recovery force vectors. The nondimensional dynamic pressure λ as defined from Eq. (2),

$$\lambda = \frac{2qa^3}{D_{110}\sqrt{M_\infty^2-1}}, \tag{25}$$

where $D = D_{110}$ is the D_{11} of the composite material (V_m=1) with all fibers aligned in 0^0 or x-direction. The aerodynamic damping from Eq. (2) is

$$g_a = \frac{\rho_a V_\infty (M_\infty^2-2)}{\rho h \omega_o (M_\infty^2-1)^{3/2}} \tag{26}$$

1C. Solutions

The equation of motion, Eq. (24), is a set of ordinary differential equations with respect to time t. However, the force vectors $\{P_{\Delta T}\}$ and $\{P_\sigma\}$ are time independent. Thus the total solution is

$$\{W\} = \{W\}_s + \{W\}_t, \tag{27}$$

where $\{W\}_s$ is the time-independent particular solution which yields the aerothermal postbuckling deflection with SMA recovery stress effect, whereas $\{W\}_t$ is the time-dependent homogeneous solution of linear flutter motions. Substituting Eq. (27) into Eq. (24), the following two equations are obtained:

$$(\lambda[A_a]+[K]-[K_{N\Delta T}]+[K_\sigma]+\tfrac{1}{2}[N1]_s+\tfrac{1}{3}[N2]_s)\{W\}_s = \{P_{\Delta T}\}-\{P_\sigma\} \tag{28}$$

$$\frac{1}{\omega_o^2}[M]\{\ddot{W}\}_t + \frac{g_a}{\omega_o}[G]\{\dot{W}\}_t + (\lambda[A_a]+[K]-[K_{N\Delta T}]+[K_\sigma]+[N1]_s+[N2]_s)\{W\}_t = 0. \tag{29}$$

The Newton-Raphson iteration method is well suited to determine $\{W\}_S$ from Eq. (28), and the coalescence of the lowest two modes determines the critical dynamic pressure from Eq. (29). Detailed solution procedures are referred to Refs. [7, 8].

2. Numerical Results and Discussions

A simply supported SMA fiber embedded $[0/45/-45/90]_S$ graphite-epoxy square panel (a=b=12 in, h=0.05 in) is studied. The SMA fibers are homogeneous throughout the panel in the same directions as of the graphite fibers. The material properties of the graphite-epoxy and SMA fiber are shown in Appendix.

It is known that the recovery stress σ_r^* (see Fig. 11) is a nonlinear function of the temperature and the initial strain, at high temperatures it remains almost unchanged. At 180 °F, the recovery stress can be calculated from the expression [17]

$$\sigma_r^* = 5.34 \times 10^6 \varepsilon_r^3 - 4.89 \times 10^5 \varepsilon_r^2 + 1.68 \times 10^4 \varepsilon_r \quad (MPa), \quad \varepsilon_r < 5\%. \tag{30}$$

In the finite-element results, it is assumed that the recovery stress is constant and can be calculated from Eq. (30) when $T > A_f$.

2A. Critical Buckling Temperature and Thermal Postbuckling

Tables 2 shows the critical buckling temperatures and the maximum thermal postbuckling deflections of the $[0/45/-45/90]_S$ graphite-epoxy composite panel embedded with SMA fibers of various initial strains and volume fractions. It is observed that for $T > A_f$ the buckling temperatures increase with increasing volume fraction and with increasing initial strain of the SMA fibers. At low temperatures ($T < A_S$), the critical temperature is decreased with the increasing of SMA volume fraction, because $E_s^* < E_{1_m}$. Large thermal postbuckling deflection could alter the aerodynamic flow field and thus reduce the operation performance and efficiency of the aircraft as well as significantly increase surface temperatures. The elimination or reduction of the thermal postbuckling deflection by embedded SMA fibers will maintain the original optimal aerodynamic performance designed for the aircraft.

Figures 12 and 13 show that the flutter stability region is enlarged significantly at high temperatures ($T > A_f$) with the increase of SMA fiber volume fraction and initial strain. Figure 14 shows that the stability region decreases slightly at low temperatures ($T < A_S$) when the panel has more SMA fibers because $E_s^* < E_{1_m}$ as previously noted.

Table 2 Critical Buckling Temperatures ΔT_{cr} (°F)

SMA Vol. Vs (%)	$T < A_s$	$T > A_f$		
		$\varepsilon_r = 2\%$	$\varepsilon_r = 3\%$	$\varepsilon_r = 4\%$
0	21.4	-	-	-
10	18.7	152	169	185
20	16.3	314	354	390
30	14.3	523	591	653

In the transient temperature range ($A_s < T < A_f$), only part of the total initial strain can be recovered, and the recovery stress can not be estimated from Fig. 11. Detailed calculations showed that the critical dynamic pressure increases linearly with the temperature, and the stability boundary is a straight line between (A_s, λ_s) and (A_f, λ_f). Figure 15 shows the complete flutter stability boundaries for the composite panel studied with SMA ($V_s=0.2$, $\varepsilon_r=0.03$) and without SMA ($V_s=0$). This certainly demonstrates that SMA can greatly enlarge the stable region especially at high temperatures.

V. INTEGRATED INTELLIGENT STRUCTURE

In sections III and IV, the use of piezoelectric material and shape memory alloy (SMA) to suppress panel flutter motions have been investigated, respectively. The dynamic equations of motion have been derived. The primary results for isotropic as well as composite panels are obtained. If limit-cycle flutter motions occur, they can be suppressed quickly within the critical dynamic pressure with piezoelectric actuators (Fig. 3). The flutter boundary is increased tremendously at high temperatures with the use of SMA. Therefore, it is suggested that the piezoelectric materials are to be used to actively suppress the panel flutter at the low temperatures ($T < A_s$) since the SMA will not be activated in this region. On the other hand, the SMA should be adopted to enlarge the stability flight envelope at the high temperatures ($T > A_f$).

In this section, both piezoelectric material and SMA are embedded in the same laminated composite panel. SMA fibers are aligned in the same direction as the graphite fibers in each composite lamina. The finite element time domain approach is adopted in this study.

Finally, consider the example of a panel with only 20% SMA fibers embedded in the composite laminate and residual strain taken to be 3%, and with embedded piezo of dimension 2.4"x8" at the leading edge. The critical dynamic pressures are shown in Fig. 16 for the panel at various temperatures. By using integrated SMA and piezo, the stability
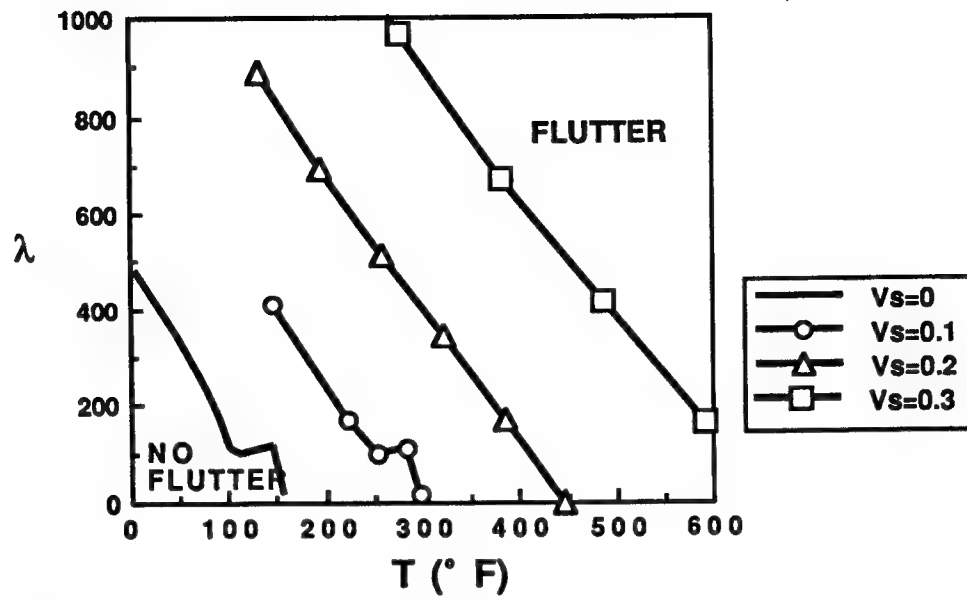
Fig. 12 Flutter stability boundaries of SMA/composite plates (ε_r=0.02) with different SMA volume fractions
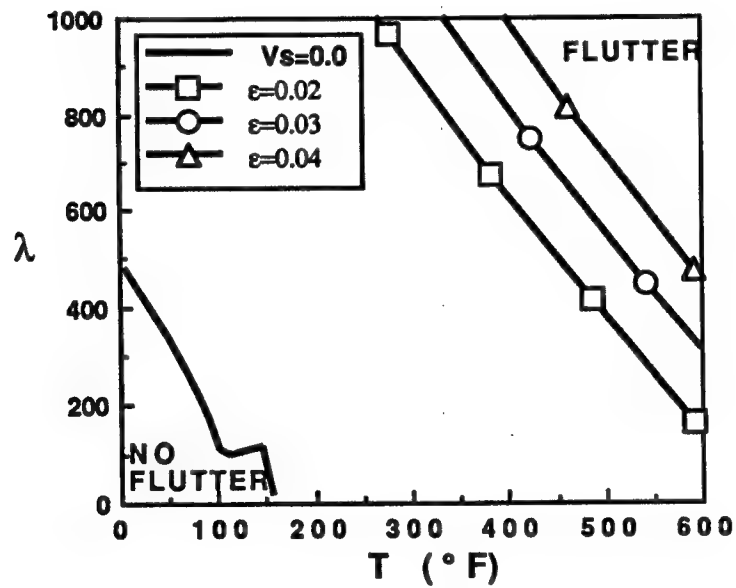

Fig. 13 Flutter stability boundaries of SMA/composite plates (V_s=0.3) with different initial recovery strains
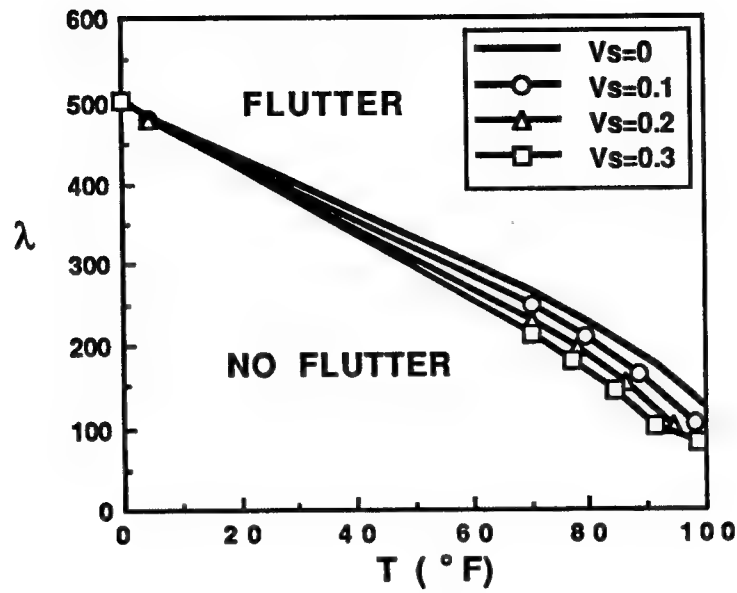
Fig. 14 Flutter stability boundaries of SMA/composite plates with different SMA volume fractions at low temperatures (T<A$_S$)
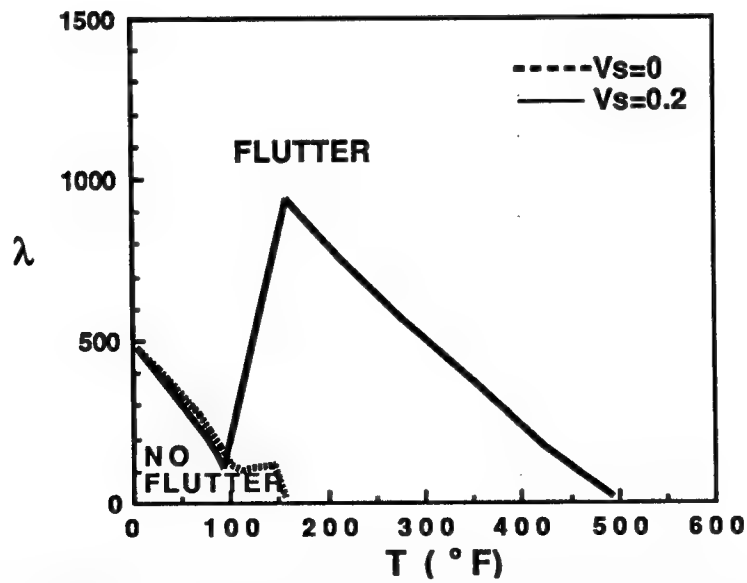

Fig. 15 Complete stability boundary for SMA/composite panel with ε_r=0.03.
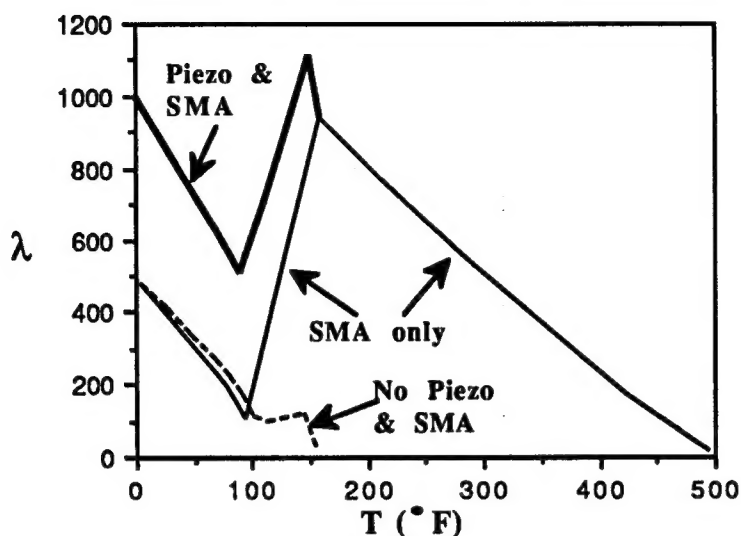
Fig. 16 Complete stability boundary for a composite panel with or without piezo and SMA(V_s=0.2 and ε_r=0.03).

boundary is enlarged throughout the temperature range. The critical dynamic pressure is therefore increased. When T<A_s, the SMA is not active. On the other hand, when T>A_s, SMA is automatically activated, but with relatively small recovery stress. When T>A_f, the large recovery stresses will stiffen the panel so that the critical dynamic pressure is further increased. In this region, the passive control using SMA is automatically achieved. In this study, however, the piezoelectric materials are assumed to be independent of temperatures. The effect of temperature on piezoelectric material will be included in Phase II.

VI. CONCLUSION

The ultimate goal of this project is to develop a commercial package of methodology, information, and criteria, along with documented computer programs, for designing integrated intelligent panel structures to meet static aerothermoelastic deformation and flutter requirements. To accomplish this we have, in Phase I, investigated the properties and behaviors of integrated intelligent structures consisting of advanced composite laminates, embedded shape memory alloys (SMA) and piezoelectric materials, and two dynamic control systems.

The fundamental conclusion of this Phase I effort is that it is possible to use existing technology to develop the proposed innovative integrated intelligent structure to meet static

aerothermoelastic deformation and flutter requirements and to systemize the process of designing such structures to meet specified requirement. Panel flutter suppression can be achieved for integrated intelligent composite structure by using piezoelectric materials at low temperatures and SMA at high temperatures. Optimal shaped piezoelectric actuator configuration design shows that actuating a small piezoelectric layer patched adjacent to the leading edge can suppress the flutter effectively. The model-independent signature-based controller using collocated sensor/actuator is very simple and easy to implement as an effective active controller. With embedded SMA fibers, the critical buckling temperature of the composite panel is increased 10 to 20 times as compared to panel with no SMA and the flutter stability region can be enlarged significantly.

Under Phase I, we have demonstrated the feasibility of all the critical design and nonlinear analysis of the innovative intelligent structure for integration in Phase II into designing of a realistic aircraft intelligent panel for ultimate laboratory and wind tunnel testings. The extensive experience of methodology, design and analysis we have available will enable us to develop integrated intelligent panel structures to meet static aerothermoelastic deformation and flutter requirements and respond to future requirements.

By successfully meeting and exceeding all of the Phase I objectives, we have demonstrated an innovative solution to an existing need for suppressing static aerothermoelastic deformations and flutter of panels. In this way, Phase I has served its purpose as a design, analysis and demonstration period and paved the way for complete laboratory and wind tunnel testing in Phase II. The far reaching implications of the intelligent structure introduce new possibilities in both the government and commercial arenas. It is these areas which will allow widespread development and dissemination of the intelligent structure and a commercial package for its design under Phase III and hence fulfill the goals of the SBIR program.

LIST OF PUBLICATIONS

1   Lai, Z., Xue, D.Y., Huang, J.-K. and Mei C., "Nonlinear Panel Flutter Suppression with Piezoelectric Actuation," Proceedings of the Second Conference on Recent Advances in Active Control of Sound and Vibration, Blacksburg, VA, April 28-30, 1993, pp. 863-874.

2   Lai, Z., Zhou, R. C., Xue, D.Y., Huang, J.-K. and Mei C., "Suppression of Panel Flutter at Elevated Temperature with Piezoelectric Actuator," Proceedings of AIAA 34th Structures, Structural Dynamics and Materials Conference, La Jolla, CA, April 19-21, 1993, pp. 3466-3474.

3   Xue. D. Y. and Mei, C., "A Study of the Application of Shape Memory Alloy in Panel Flutter Control," Accepted for Presentation at the 5th International Conference on

Recent Advances in Structural Dynamics, Institute of Sound and Vibration Research, Univ. of Southampton, Southampton, UK, July 18-21, 1994.

4 Zhou, R. C., Hsiao, M.-H., Xue, D.Y., Lai, Z., Mei C., and Huang, J.-K., "Nonlinear Flutter Control of Composite Panels with Embedded Piezoelectric Materials Using Finite Element Method," To Appear in the Proceedings of AIAA 35th Structures, Structural Dynamics and Materials Conference, Hilton Head, SC, April 18-20, 1994.

REFERENCES

1 Jordan, P. F., "The Physical Nature of Panel Flutter," Aero Digest, February 1956, pp. 34-38.

2 Bisplinghoff, R. L. and Ashley, H., *Principles of Aeroelasticity*, John Wiley, 1962, pp. 419.

3 Baker, R., "F-117A Structures and Dynamics Design Considerations," Plenary Session 8, AIAA Dynamics Specialist Conference, Dallas, TX, April 16-17, 1992.

4 Schaeffer, H. G. and Heard, W. L., Jr., "Flutter of a Flat Plate Exposed to a Nonlinear Temperature Distribution," AIAA Journal, 3, 1965, pp. 1918-1923.

5 Yang, T. Y. and Han, A. D., "Flutter of Thermally Buckled Finite Element Panels," AIAA Journal, 14, 1976, pp. 975-977.

6 Xue, D. Y. and Mei, C., "Finite Element Nonlinear Flutter and Fatigue Life of Two-Dimensional Panels with Temperature Effects," Proceedings of 32nd Structures, Structural Dynamics and Materials Conference, Baltimore, MD, April 1991, pp. 1971-1980.

7 Xue. D. Y. and Mei, C., "Finite Element Nonlinear Panel Flutter with Arbitrary Temperatures in Supersonic Flow," AIAA Journal, Vol. 31, 1993, pp. 154-162.

8 Dixon, I. R. and Mei, C., "Nonlinear Flutter of Rectangular Composite Panels under Uniform Temperature using Finite Elements," In Nonlinear Vibrations, DE-Vol. 50 and AMD-Vol. 144, ASME Winter Annual Meeting, Anaheim, CA, November 1992, pp. 123-132.

9 Lai, Z., Xue, D.Y., Huang, J.-K. and Mei C., "Nonlinear Panel Flutter Suppression with Piezoelectric Actuation," Proceedings of the Second Conference on Recent Advances in Active Control of Sound and Vibration, Blacksburg, VA, April 28-30, 1993, pp. 863-874.

10 Lai, Z., Zhou, R. C., Xue, D.Y., Huang, J.-K. and Mei C., "Suppression of Panel Flutter at Elevated Temperature with Piezoelectric Actuator," Proceedings of AIAA 34th Structures, Structural Dynamics and Materials Conference, La Jolla, CA, April 19-21, 1993, pp. 3466-3474.

11 Juang, J.-N., Wu, S.-C., Phan, M. and Longman, R. W., "Passive Dynamic Controllers for Nonlinear Mechanical Systems," Proceedings of AIAA 32nd Structures, Structural Dynamics and Materials Conference, Baltimore, MD, April 8-10, 1991, pp. 2640-2653.

12 Jackson, C. M., Wagner, H. J. and Wasilewski, R. J., "55-Nitinol-The Alloy with a Memory: Its Physical Metallurgy, Properties and Applications," NASA CP-5110, 1972.

13 Dowell, E. H., "Panel Flutter: A Review of the Aeroelastic Stability of Plates and Shells," AIAA Journal, 8, 1970, pp. 385-399.

14 Liang, C., Rogers, C. A. and Fuller, C. R., "Acoustic Transmission and Radiation Analysis of Adaptive Shape Memory Alloy Reinforced Laminated Plates," Journal of Sound and Vibration, Vol. 15, 1991, pp. 23-41.

15 Rogers, C. A., Liang, C. and Jia, J., "Behavior of Shape Memory Alloy Reinforced Composite Plates - Part I and II," Proceedings of the 30th Structures, Structural Dynamics and Materials Conference, Mobile, AL, 1989, pp. 2011-20.

16 Xue. D. Y. and Mei, C., "A Study of the Application of Shape Memory Alloy in Panel Flutter Control," Accepted for Presentation at the 5th International Conference on Recent Advances in Structural Dynamics, Institute of Sound and Vibration Research, Univ. of Southampton, Southampton, UK, July 18-21, 1994.

17 Cross, W. B. and Stimler, F. J., "Nitinol Characterization Study," NASA CR-1433, 1969.

APPENDIX

Properties of Panel Used in Calculations

Isotropic Panel (see Figure 1)

$a = 12$ in

$b = 12$ in

$h = 0.08$ in

$h_b = 0.05$ in

$E_b = 1.0 \times 10^7$ psi

$v_b = 0.3$

$\rho_b = 0.2588 \times 10^{-3}$ lb-s^2/in^4

Piezoelectric Material

$\alpha_p = 3.0 \times 10^{-6}/\text{°F}$

$d_{31} = d_{32} = -7.48 \times 10^{-9}$ in/v

$e_{3max} = 1.52 \times 10^4$ v/in

$h_p = 0.015$ in

$E_p = 9.0 \times 10^6$ psi

$v_p = 0.3$

$\rho_p = 0.7101 \times 10^{-3}$ lb-s^2/in^4

Graphite/Epoxy Panel

$E_{1m} = 22.5E+6$ psi

$E_{2m} = 1.17E+6$ psi

$G_{12m} = 0.66E+6$ psi

$v_{12m} = 0.22$

$\rho_m = 0.056$ lb/in^3

$\alpha_{1m} = -0.04E-6$ /°F

$\alpha_{2m} = 16.7E-6$ /°F

SMA-Nitinol

$E_s^* = 3.996E+6$ psi,   (T<As)

$E_s^* = 11.994E+6$ psi, (T>Af)

$G_s^* = 3.604E+6$ psi,   (T<As)

$G_s^* = 3.712E+6$ psi,   (T>Af)

$\rho_s = 0.2325$ lb/in^3, $v_s = 0.3$

$A_S = 100$ °F, $A_f = 145$ °F

$\alpha_S = 5.7E-6$ /°F, $\varepsilon_r = 2\sim4\%$